JOURNAL OF Materials CHEMISTRY

Formation and migration of cation defects in the perovskite oxide $LaMnO_3$

Roger A. De Souza,*[a]† M. Saiful Islam[b] and Ellen Ivers-Tiffée[a]

[a]*Institut für Werkstoffe der Electrotechnik, Universität Karlsruhe, Adenauerring 20, D-76131 Karlsruhe, Germany*
[b]*Department of Chemistry, University of Surrey, Guildford, Surrey, UK GU2 5XH*

Received 24th February 1999, Accepted 28th April 1999

Atomistic simulation techniques have been employed to investigate the energetics of cation formation and migration in cubic, rhombohedral and orthorhombic $LaMnO_3$. The calculations suggest that for rhombohedral and orthorhombic lanthanum manganite, oxidative nonstoichiometry leads to the formation of cation vacancies on both La and Mn sites, though tending towards more La vacancies. The activation energy for lanthanum vacancy migration was found to increase with departure from cubic perovskite symmetry in the order: cubic < rhombohedral < orthorhombic. A number of different pathways for manganese vacancy migration were examined. The lowest energy pathway was found to be a curved path between Mn sites that are adjacent along the $<100>_{cubic}$ directions. Calculated migration energies for this path also increased with distortion from the cubic form. The effect of composition on cation migration energies was also examined.

1 Introduction

The series of compounds based on $LaMnO_3$ are some of the most fascinating members of the perovskite oxide family, due to the variety of interesting physical properties that they display. The parent compound first attracted attention almost fifty years ago,[1] but widespread interest in this system was generated first by the emergence of strontium-doped lanthanum manganite as the cathode material of choice for the solid oxide fuel cell (SOFC)[2] and, more recently, by the discovery of colossal magnetoresistance (CMR) in those compounds with mixed Mn valence.[3,4]

In both of these fields of research the defect chemistry and the oxygen nonstoichiometry are of considerable importance. It is well known that lanthanum manganite is somewhat unusual in comparison to most other perovskite oxides in that it exhibits oxidative nonstoichiometry. The amount of excess oxygen, δ in $LaMnO_{3+\delta}$, is dependent on temperature and oxygen partial pressure.[5,6] Numerous neutron powder diffraction (NPD) studies have all indicated that cation vacancies, rather than oxygen interstitials, are responsible for the oxygen hyperstoichiometry.[7–11] However, there is some disagreement in the literature concerning the ratio of La vacancies to Mn vacancies; the most favoured descriptions are shown in Table 1.

The aim of this paper is to employ atomistic simulation techniques to investigate firstly the nature of the oxidative nonstoichiometry and secondly the migration of cation defects in this system. Cation migration plays an important role in the fabrication and processing of oxide ceramics, and also in the reverse process of degradation. The long term behaviour of devices incorporating such materials may depend on them maintaining their structure under mechanical load (creep) and their chemical composition under (electro-) chemical potential gradients (kinetic demixing, interdiffusion).

To date there have been no reports in the literature concerned with the direct determination of cation diffusion coefficients in the $LaMnO_3$ system. Information has been obtained, however, by investigating some of the processes mentioned above, *i.e.* processes that depend upon the solid state migration of cation defects. For instance, several groups have studied the sintering of $La_{1-x}Sr_xMnO_{3+\delta}$ powder compacts. Although the results from the various groups are all fairly consistent, two different explanations have been advanced. Katayama *et al.*[12] and Hammouche *et al.*[13] independently came to the same conclusion that the Mn^{4+} concentration determines the sintering behaviour, although the exact mechanism was not elucidated. In contrast, van Roosmalen *et al.*[14] and Stevenson *et al.*[15] both asserted that A-site diffusion is the rate limiting process for sintering. Quantitative information about cation transport has been obtained from a study by Wolfenstine *et al.* of the creep of $La_{1-x}Sr_xMnO_{3+\delta}$ ceramics.[16] They reported that the activation energy for creep decreased with Sr content from 490 kJ mol^{-1} for $La_{0.9}Sr_{0.1}MnO_{3+\delta}$ to 460 kJ mol^{-1} for $La_{0.75}Sr_{0.25}MnO_{3+\delta}$ and proposed that the deformation of the ceramics was controlled by lattice diffusion of one of the cations. Interestingly, there is some evidence of cation migration in a microstructural study by Weber *et al.* of $La_{0.8}Sr_{0.2}MnO_{3+\delta}$ SOFC cathodes that had been operated at 950 °C for *ca.* 2000 h.[17] It was observed that considerable changes, such as grain growth, densification and migration of Mn out of the cathode and into the electrolyte, had taken place. These degradation processes are all indicative of cation transport.

Table 1 Favoured descriptions of cation site occupancies as determined from neutron powder diffraction studies

Model	Description	Reference
(i)	$[V'''_{La}] > [V''_{Mn}]$	7, 9
(ii)	$[V'''_{La}] = [V''_{Mn}]$	8, 11
(iii)	$[V'''_{La}] < [V''_{Mn}]$	10

2 Simulation methodology

The computational techniques used in this work, embodied in the GULP code,[18] are well established and have been reviewed in detail elsewhere.[19,20] Hence, only a brief summary is given here.

The calculations are based upon the Born model of ionic solids with ions assigned integral charges corresponding to their formal oxidation states. The interactions between the

†Current address: Max-Planck-Institut für Festkörperforschung, Heisenbergstr. 1, D-70569 Stuttgart, Germany.
E-mail: desouza@chemix.mpi-stuttgart.mpg.de.

ions are formulated in terms of long range Coulombic forces and short range forces that account for electron cloud overlap (Pauli repulsion) and dispersion (van der Waals) interactions. The short range interactions are modelled with a Buckingham potential [eqn. (1)];

$$V_{ij}(r) = A_{ij} \exp\left(-\frac{r}{\rho_{ij}}\right) - \frac{C_{ij}}{r^6} \quad (1)$$

where A_{ij}, ρ_{ij} and C_{ij} are empirically derived parameters. Short range interactions are negligible beyond several lattice units, and were therefore set to zero beyond 12 Å in order to reduce computation time.

The accurate calculation of defect energies requires ionic polarisability to be included. This is incorporated by means of the shell model[21] which treats such effects in terms of a shell with charge Y connected to a core with charge $Z-Y$, where Z is the formal charge of the ion, by an isotropic harmonic spring of force constant k. The potential and shell model parameters used in this work are listed in Table 2. They are taken from the earlier study of oxygen migration in these materials by Cherry *et al.*,[22] with the exception of the $Mn^{4+}\cdots O^{2-}$ interaction which was taken from the study of lithium manganate spinels by Ammundsen *et al.*[23]

The calculation of defect formation and migration energies utilised the Mott–Littleton approach, in which the crystal lattice is partitioned into two regions: a spherical inner region with the defect at its centre (Region I) and an outer region which extends to infinity (Region II). In Region I, which contained between 150 and 200 ions, interactions are calculated explicitly so that the response of the lattice to the defect is modelled by relaxing the positions of these ions to zero force. For the remainder of the crystal (Region II), the forces due to the defect are relatively weak, and therefore the response can be treated by more approximate quasi-continuum methods. The migration energy of an ion was determined by calculating the defect energy of the migrating ion at different points along the migration path. At the position of maximum energy, the energy of the migration ion was also calculated in a direction perpendicular to the migrating route in order to confirm that a true saddle point had been found. This approach also yields the saddle point configuration, from which the energy barrier to migration is derived, and is most reliable for systems in which the energy surface is symmetrical.

The GULP code also allows fractional occupancies to be specified for crystallographic sites. Thus it was possible to model crystals with random distributions (as opposed to ordered arrangements) of cations defects (acceptor dopants) and compensating defects (electron holes). This is implemented through a mean field approach: the site in question is assumed to contain a hybrid ion, for which the short range interaction energy takes the form of eqn. (2), *e.g.* for partial substitution of La by Sr:

$$V_{A^{(3-x)+}\cdots O^{2-}} = xV_{Sr^{2+}\cdots O^{2-}} + (1-x)V_{La^{3+}\cdots O^{2-}} \quad (2)$$

The calculation of defect energies in the acceptor-doped compositions required corrections to be made in order to account for the existence of hybrid cations.

Table 2 Potential parameters for $LaMnO_3$

(a) Short range potential

Interaction	A/eV	ρ/Å	C/eV Å^6
$La^{3+}\cdots O^{2-}$	1545.21	0.3590	0
$Mn^{3+}\cdots O^{2-}$	1267.50	0.3214	0
$Mn^{4+}\cdots O^{2-}$	1345.15	0.3180	0
$Sr^{2+}\cdots O^{2-}$	959.1	0.3721	0
$O^{2-}\cdots O^{2-}$	22764.3	0.1490	43.0

(b) Shell model

Species	Y/e	k/eV Å^{-2}
La^{3+}	−0.25	145
Mn^{3+}	3.00	95
Mn^{4+}	4.00	95
Sr^{2+}	3.25	71.7
O^{2-}	−2.24	42.0

3 Results and discussion

3.1 Perfect lattice calculations

The crystal structure of lanthanum manganite is dependent on the amount of excess oxygen. Experimentally, orthorhombic symmetry (*Pbnm*) is observed up to $\delta = 0.105$, while for higher values of δ, rhombohedral symmetry ($R\bar{3}c$) is seen,[24] at least up to $\delta = 0.29$.[10] In the present study it was possible to reproduce the rhombohedral[10] and orthorhombic[25] structures, as well as an idealised cubic structure ($Pm\bar{3}m$), with the same set of potential parameters. Calculated crystal data are presented in Table 3. It is emphasised that δ is zero for the perfect lattice simulations of all three systems.

We note that perfect agreement is seen between calculated and experimental cubic lattice parameters, because Cherry *et al.* derived the empirical parameters for $LaMnO_3$ by fitting to this structure.[22] Although the other two structures are not exactly reproduced, we are interested in separating the effects of symmetry from those of composition. For this purpose the fact that all three systems can be modelled is sufficient. We are aware that crystal field effects are not explicitly included; however, since the structures are reproduced, such effects are, to some degree, implicitly incorporated.

3.2 Frenkel and Schottky disorder

The energies of isolated vacancy and interstitial defects were computed for the rhombohedral and orthorhombic structures. We considered two possible interstitial sites in the perovskite structure: the octahedral interstice at $(0,0,1/2)_{cubic}$ and the tetrahedral interstice at $(1/4,1/4,1/4)_{cubic}$; in all cases lower energies were found for interstitials placed in the octahedral site and thus only these were employed in the calculations detailed below. In addition we mention that there are two oxygen sites in the orthorhombic structure and hence two oxygen vacancy energies; the difference in energy between the two values was rather small (0.02 eV), which may possibly reflect the calculated orthorhombic structure being less distorted than the experimentally observed structure.

Frenkel disorder, full Schottky disorder and partial Schottky disorder energies were calculated by combining the individual defect energies (and including lattice energies where appropriate). These defect reactions are given below [eqn. (3)–(8)] and the corresponding energies listed in Table 4. To enable comparisons between the two types of disorder reactions, the energies are given as effective defect formation energies, *i.e.* $E_F/2$ for Frenkel disorder and $E_S/5$ for Schottky disorder.

Lanthanum Frenkel disorder:

$$La_{La}^{x} \rightarrow V_{La}''' + La_i^{\cdots} \quad (3)$$

Manganese Frenkel disorder:

$$Mn_{Mn}^{x} \rightarrow V_{Mn}''' + Mn_i^{\cdots} \quad (4)$$

Oxygen Frenkel disorder:

$$O_O^{x} \rightarrow V_O^{\cdot\cdot} + O_i'' \quad (5)$$

$LaMnO_3$ full Schottky disorder:

$$\text{'nil'} \rightarrow V_{La}''' + V_{Mn}''' + 3V_O^{\cdot\cdot} + LaMnO_3^{surf} \quad (6)$$

Table 3 Calculated lattice properties for $LaMnO_3$ crystals

	Cubic $Pm\bar{3}m$	Rhombohedral $R\bar{3}c$	Orthorhombic $Pbnm$
Lattice energies/eV	−139.69	−139.84	−139.87
Unit cell parameters:			
a/Å	3.904 (3.904)	5.541 (5.522)[a]	5.528 (5.582)[b]
b/Å	—	—	5.553 (5.583)[b]
c/Å	—	13.511 (13.332)[a]	7.818 (7.890)[b]
Dielectric constants:			
Static, $<\varepsilon_0>$	52.71	33.54	18.69
High frequency, $<\varepsilon_\infty>$	2.16	2.18	2.19

Experimental values in parentheses: [a]ref. 10; [b]ref. 25.

Table 4 Calculated energies for Frenkel disorder, partial Schottky disorder and full Schottky disorder in $LaMnO_3$ crystals

		Energy/eV per defect	
Reaction	Eqn.	Rhombohedral	Orthorhombic
La Frenkel	(3)	10.08	9.25
Mn Frenkel	(4)	8.79	9.19
O Frenkel	(5)	4.02	4.00
$LaMnO_3$ full Schottky	(6)	3.48	3.73
La_2O_3 partial Schottky	(7)	3.20	3.50
Mn_2O_3 partial Schottky	(8)	3.72	3.94

La_2O_3 partial Schottky disorder:

$$\text{'nil'} \rightarrow 2V'''_{La} + 3V^{\cdot\cdot}_{O} + La_2O_3{}^{surf} \quad (7)$$

Mn_2O_3 partial Schottky disorder:

$$\text{'nil'} \rightarrow 2V'''_{Mn} + 3V^{\cdot\cdot}_{O} + Mn_2O_3{}^{surf} \quad (8)$$

For both systems the cation Frenkel disorder energies are much higher than the other disorder energies. The oxygen Frenkel energies are comparable to the Schottky disorder energies, but it is likely that the former are underestimates of the true values. This is possibly due to the use of an empirical $O^{2-}\cdots O^{2-}$ potential which may result in a more favourable energy for the oxygen interstitial. Nevertheless, this interatomic potential has been employed successfully in a range of studies on oxygen defect formation and migration in other oxide materials.[20,22,26]

We can therefore conclude that vacancies, and not interstitials, will be the dominant structural defects. This is to be expected from the close-packed nature of the perovskite lattice, and is consistent with NPD work.[7–11] However, the Schottky energies are so high that we would not expect intrinsic disorder to dominate the defect chemistry, except at very high temperatures. We note that the disorder energies increase on going from the rhombohedral system to the orthorhombic system.

3.3 Oxidative nonstoichiometry

As mentioned earlier, there is a lack of consensus between NPD studies as to the distribution of cation vacancies over the two cation sub-lattices in oxygen excess compositions. Consequently we have examined the energetics of three different oxidation reactions [eqn. (9)–(11)]:

$$3/2O_2 \rightarrow 2V'''_{La} + 6h^{\cdot} + La_2O_3 \quad (9)$$

$$3/2O_2 \rightarrow V'''_{La} + V'''_{Mn} + 6h^{\cdot} + LaMnO_3 \quad (10)$$

$$3/2O_2 \rightarrow 2V'''_{Mn} + 6h^{\cdot} + Mn_2O_3 \quad (11)$$

The electron hole state was modelled as a Mn^{4+} ion (*i.e.* as a small polaron), although we acknowledge that the hole state in lanthanum manganite exhibits mixed Mn 3d and O 2p character;[27] the emphasis here was not on the character of the electron hole but rather on the nature of the oxidative nonstoichiometry. In order to calculate the reaction energies of eqns. (9)–(11), we require, in addition to the individual defect energies and the lattice energies, the dissociation energy of an oxygen molecule (5.16 eV), the first and second electron affinities of oxygen (−1.46 and +8.75 eV respectively) and the fourth ionisation energy of manganese (52 eV).[28] We are aware that the second electron affinity of oxygen[29] and the ionisation energies of a cation vary according to the composition and structure of an oxide, and therefore that the use of free-ion energies for these quantities, in the absence of experimentally or theoretically accessible values for either $LaMnO_3$ structure, will introduce significant uncertainty into the redox reaction energies. However, we stress that the trend seen for a particular structure will still be valid. In addition we note that this approach to calculating redox energies has been successfully applied to other transition metal oxides including the cuprate superconductors.[26,30] The merit of this approach is that it includes detailed estimates of lattice relaxation and Coulomb energies which are difficult to obtain from other methods.

The calculated reaction energies are listed in Table 5. We will first consider the results for rhombohedral lanthanum manganite. The energies for reactions (9) and (10) are similar, which suggests that both lanthanum and manganese vacancies will be present in rhombohedral $LaMnO_{3+\delta}$ (*i.e.* $\delta > 0.105$), but that there will be a tendency towards more lanthanum vacancies. In other words, Model (i) of Table 1 provides the correct description of rhombohedral $LaMnO_{3+\delta}$. This finding is in agreement with the NPD studies of Tofield and Scott[7] and Mitchell *et al.*[9] For those NPD studies in Table 1 in which Model (ii) was proposed,[8,11] it should be emphasised that the preference for Model (ii) over Model (i) was based on no second phase, such as Mn_2O_3 (Mn_3O_4) or La_2O_3, being observed. This brings us to the question of why no La_2O_3 second phase has been observed experimentally, if Model (i) is correct. Tofield and Scott suggested that lanthanum hydroxides, being poorly crystalline, may evade detection by X-ray diffraction,[7] although van Roosmalen *et al.* did not detect any second phases even using high resolution TEM.[8] Tofield and Scott also considered the possibility of antisite defects (La_{Mn}^{x}) being involved in oxidative nonstoichiometry,[7] but we can discount this explanation, as the calculated energies for such reactions are *ca.* 5 eV higher than the energies for reactions (9)–(11). Nevertheless, there is further, independent support for Model (i) which comes from a study of the La_2O_3–Mn_2O_3 phase diagram[31] in which it was reported that the lanthanum

Table 5 Calculated energies for oxidation reactions in $LaMnO_3$ crystals

	Energy/eV per hole	
Eqn.	Rhombohedral	Orthorhombic
(9)	5.19	5.51
(10)	5.43	5.71
(11)	5.63	5.88

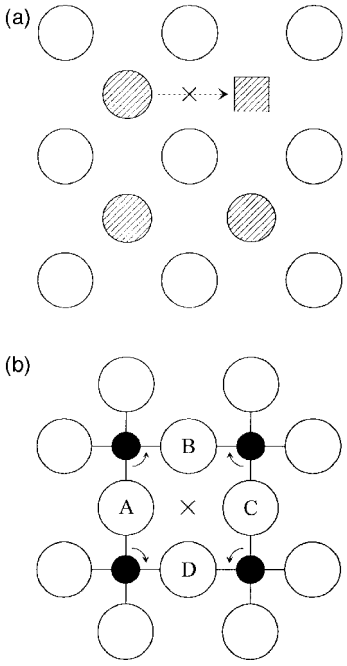

Fig. 1 (a) Schematic diagram of the investigated $<100>_{cubic}$ path for La migration. (b) Schematic diagram of the octahedral interstice, seen in the direction of migration. The small filled circles are Mn cations, the larger line-shaded circles are La cations, the large open circles are oxygen anions and the cross denotes the saddle point.

manganite perovskite phase exists up to higher La deficiency than Mn deficiency.

For the orthorhombic system, our results indicate that Model (i) applies to this structure as well. In contrast Mitchell *et al.* found that the Mn site was fully occupied and hence that only La vacancies are present in orthorhombic $LaMnO_3$.[9] This would appear to suggest that the oxidation reaction (9) should have a much lower energy relative to reaction (10). The reason for this discrepancy is at present not clear.

3.4 Cation vacancy migration

3.4.1 Effect of symmetry. It is apparent upon examination of the perovskite structure that lanthanum diffusion is most likely to take place by vacancy migration in the $<100>_{cubic}$ directions [Fig. 1(a)]. Therefore a lanthanum vacancy can change places with one of six lanthanum ions. In the cubic and rhombohedral crystal structures of $LaMnO_3$, all six La jump distances are equal, while in the orthorhombic structure, the displacement of La ions from their ideal cubic positions results in three different La jump distances.

The calculated activation energies for La vacancy migration, E_m^{La}, are listed in Table 6. There is a clear trend towards higher migration energies as the perovskite lattice becomes more distorted. This is because the saddle point energy increases at a higher rate across the series than does the energy of an isolated lanthanum vacancy, which suggests that the saddle point configuration should be examined more closely.

Table 6 Comparison of calculated activation energies for lanthanum vacancy migration, E_m^{La}, with the shortest oxygen–oxygen separation across the octahedral interstice, d_{O-O}^{oct}, in $LaMnO_3$ crystals

	E_m^{La}/eV	d_{O-O}^{oct}/Å
Cubic	3.93	3.904
Rhombohedral	4.14	3.481
Orthorhombic	4.22	3.469
	4.26	3.415
	4.32	3.406

Indeed, a key feature of these atomistic simulation methods is the information provided on the local lattice relaxation around defects and migrating species.

The saddle point configuration probed in these calculations consists of the migrating La ion moving through an aperture defined by the four oxygen ions of the octahedral interstice. The radius of a sphere that will just pass through this aperture is in fact equal to the radius of the B site cation for the ideal cubic perovskite structure. As the A site cation is much larger than the B site cation, the surrounding lattice must relax substantially in order to allow the A site cation to migrate. Indeed, from the simulations we found that in the saddle point configuration each of the four oxygen ions is displaced by 0.27 Å away from the migrating cation. Thus the four oxygen ions of the octahedral interstice will clearly provide severe steric hindrance to A site migration. We note that this type of steric approach has previously been applied by Kilner and Brook to oxygen ion migration in perovskites.[32]

In the non-cubic perovskite lattices, the four oxygen ions are no longer located at the corners of a square, as they are in the ideal cubic structure. Instead, due to the rotation of the BO_6 octahedra, two of the oxygen ions, situated across one of the diagonals of the square, move towards each other [oxygen ions A and C in Fig. 1(b)]; the other two, situated across the other diagonal [oxygen ions B and D in Fig. 1(b)], move away from each other (in addition the oxygen ions are no longer all in the same plane). Accordingly, we find that there is a correlation between the shortest oxygen–oxygen separation across the octahedral interstice, d_{O-O}^{oct}, and the activation energy for La migration, E_m^{La}. As expected, E_m^{La} increases as d_{O-O}^{oct} decreases, since the disturbance to the surrounding lattice is greater. This qualitative analysis is confirmed by examination of oxygen ion displacements in the saddle point configurations. As stated above, the four oxygen ions in the cubic structure are each displaced by 0.27 Å; in the non-cubic structures it was found that oxygen ions A and C are each displaced by 0.45 Å in the rhombohedral structure and by *ca.* 0.50 Å in the orthorhombic structure. Oxygen ions B and D are only displaced by 0.05 Å in the rhombohedral structure and by *ca.* 0.12 Å in the orthorhombic structure, which supports our assertion that d_{O-O}^{oct} is the critical parameter.

At first sight the obvious path for Mn migration in the perovskite lattice is between Mn sites in the $<110>_{cubic}$ directions, as illustrated in Fig. 2. The calculated migration energies for this path are extremely high, lying between 14 and 16 eV for the three structures. Examining the defect energies along the migration path yields that the saddle point is the octahedral interstice, and hence, in the transition state, the migrating Mn cation is not only surrounded by four (equatorial) oxygen anions and, more significantly, by two (apical) La cations. We therefore attribute these extremely high activation energies to electrostatic repulsion between the migrating Mn cation and the La cations.

Such high values imply that bulk Mn transport will not occur until close to the melting point of $LaMnO_3$. Given that

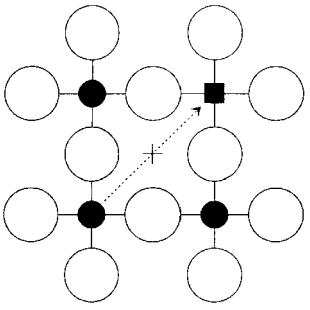

Fig. 2 Schematic diagram of the $<110>_{cubic}$ (high activation energy) path for Mn migration.

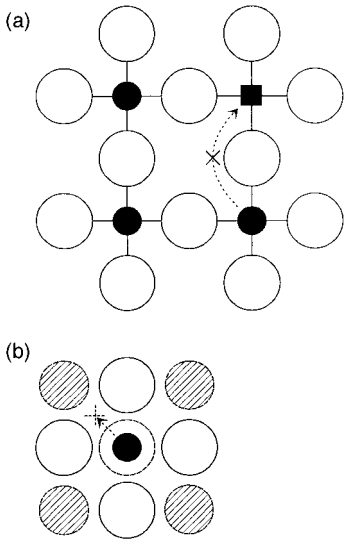

Fig. 3 Schematic diagrams of the curved, lower energy path for Mn migration. (a) Projection of the curved path onto the $\{001\}_{cubic}$ plane; (b) view in the direction of migration, $<100>_{cubic}$. Species drawn with a dotted outline (the O ion behind the Mn cation, the four lanthanum ions, and the saddle point) all lie in the plane behind the migrating Mn ion and the four oxygen ions.

the melting point for $LaMnO_3$ was reported to be 1900 °C,[33] this seems quite unreasonable. Consequently, we examined alternative pathways for manganese vacancy migration. The lowest activation energies were found for a curved migration path between Mn sites adjacent along the $<100>_{cubic}$ direction, for which the trajectory of the migrating Mn cation lies approximately in the $\{011\}_{cubic}$ plane. This is shown in Fig. 3(a) and (b): the migrating Mn cation moves up and around the oxygen ion located between the two Mn sites, which is displaced in the opposite direction and slightly downwards. In the saddle point configuration it is situated between a La cation and the intervening oxygen ion. We believe that this path represents a balance between repulsive cation interactions and the large displacement which the oxygen ion must undergo. In the cubic structure there are four equally possible quadrants for this Mn jump; in the rhombohedral structure the displacement of the oxygen ions (in particular the intervening oxygen ion) leads to one path being more favourable. In the orthorhombic structure, the location of the oxygen ion also removes the equivalence between the four possible paths; in addition, there are two different Mn jump distances.

The Mn migration energies for both paths are given in Table 7. The much lower migration energies obtained for the $<100>_{cubic}$ path compared to those obtained for the $<110>$ path are attributed primarily to a reduction in the repulsive electrostatic energy: for this migration path, the migrating Mn cation only interacts significantly with one La cation. As for lanthanum vacancy migration, the manganese vacancy migration energy ($<100>_{cubic}$ path) increases as the symmetry moves away from cubic. It might have been expected however, that E_m^{Mn} would decrease with increasing distortion on account of the rotation of the BO_6 octahedra, since the intervening oxygen ion would not have to relax as far. This suggests that the repulsive electrostatic term is still the dominant contribution.

Table 7 Calculated activation energies for manganese vacancy migration in $LaMnO_3$ crystals

	E_m^{Mn}/eV	
	$\langle 110\rangle_{cubic}$	$\langle 100\rangle_{cubic}$
Cubic	14.71	7.73
Rhombohedral	14.00, 15.73	8.82
Orthorhombic	14.11, 14.73	9.94, 10.64

For both the Mn migration paths we have ascribed the high activation energies to electrostatic repulsion between the migrating Mn cation and the neighbouring La cation(s) in the transition state. The removal of a neighbouring lanthanum cation could therefore result in a substantial reduction in migration energy. Preliminary calculations of manganese vacancy migration mediated by lanthanum vacancies yield values for E_m^{Mn} of *ca.* 3.5 eV for all three structures. We emphasise that these are tentative results, as we have only examined possible transition states, and have not evaluated the entire energy profiles for the jumps. Furthermore, one may doubt whether a lanthanum vacancy would approach a manganese vacancy so closely. Nevertheless, if this is a significant mechanism, one would expect the concentration of lanthanum vacancies to be an extremely important parameter as it would determine not only the lanthanum diffusion coefficient but also the manganese diffusion coefficient. A detailed examination of this migration mechanism and of the interaction between cation vacancies is currently being undertaken. The possible influence of oxygen vacancies on cation migration is also being considered.

A further possibility which has not been explored is that the presence of electronic defects in the vicinity of the migrating cations, for example a hole localised at a cation vacancy, may reduce the migration energies. This problem is not amenable to the atomistic simulation techniques we have used, but would be an interesting subject for an *ab initio* study.

3.4.2 Effect of composition. The compositions in the lanthanum manganite system that display the most interesting properties, and have therefore attracted the most attention, are those that are acceptor-doped on the A site with divalent cations. In this section we have investigated cation migration in Sr-doped and Ca-doped cubic systems. In both cases the divalent dopant cations were compensated for by electron holes (Mn^{4+} ions), such that $[Sr_{La}'] = [Mn_{Mn}^{\bullet}]$. In order to evaluate activation energies in such solid solutions, it was necessary to correct for hybrid cations, as noted earlier. This correction takes the form of eqn. (12), taking lanthanum vacancy migration in a Sr-doped composition as an example;

$$E_m^{La} = E(V_{La/Sr} \cdots La_m \cdots V_{La/Sr}) - E(La_{La/Sr} \cdots V_{La/Sr}) \quad (12)$$

i.e. the transition state energy minus the energy of the initial configuration.

The results for A-site migration in the acceptor-doped compositions are shown in Fig. 4. For a particular dopant level the migration energies decrease in the order $E_m^{La} > E_m^{Sr} > E_m^{Ca}$, although the ionic radius of La^{3+} in twelvefold co-ordination ($r_{La}^{XII} = 1.36$ Å) lies between those of Sr^{2+} ($r_{Sr}^{XII} = 1.44$ Å) and Ca^{2+} ($r_{Ca}^{XII} = 1.34$ Å).[34] This indicates that if we only take steric hindrance in the saddle point into consideration, we do not obtain a complete description of A-site migration, and illustrates that electrostatic and ion polarisability factors are also important. The linear increase in activation energies with increasing Mn^{4+} concentration may be due to some combination of these three factors (steric, electrostatic, ion polarisability). We note that for the compositions examined (acceptor-doped, $\delta = 0$), the activation energies for La migration depend more strongly on composition than on symmetry.

In Fig. 5 the energies for Mn^{3+} and Mn^{4+} migration along the curved path in the $<100>_{cubic}$ directions are shown. The activation energies for the migration of the smaller, but more highly charged, Mn^{4+} cation are *ca.* 2.5 eV higher than the migration energies for Mn^{3+}; this is consistent with the repulsive electrostatic interactions being dominant for this migration path. The behaviour, as a function of Mn^{4+} concen-

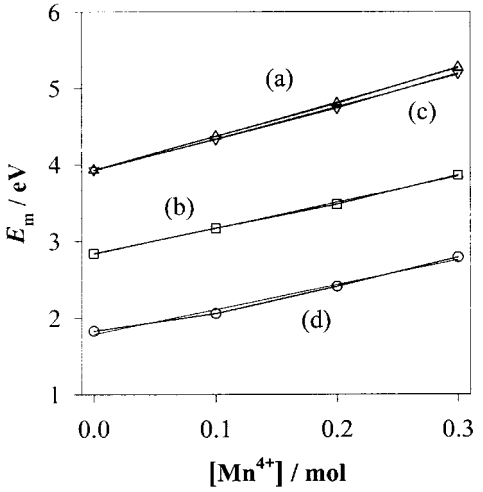

Fig. 4 Calculated activation energies for A-site migration in acceptor-doped cubic lanthanum manganite (electron hole compensation): (a) E_m^{La} ($La_{1-x}Sr_xMnO_3$), (b) E_m^{Sr} ($La_{1-x}Sr_xMnO_3$), (c) E_m^{La} ($La_{1-x}Ca_xMnO_3$), (d) E_m^{Ca} ($La_{1-x}Ca_xMnO_3$). The lines are the results of regression analysis on the data sets.

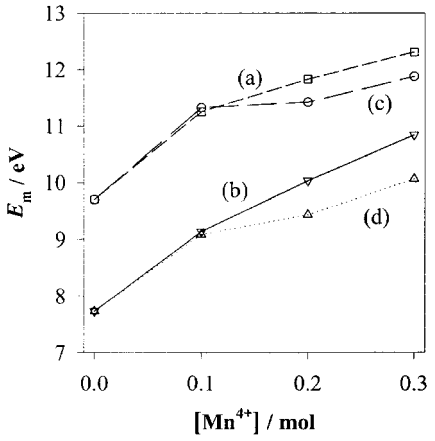

Fig. 5 Calculated activation energies for B-site migration in acceptor-doped cubic lanthanum manganite (electron hole compensation): (a) $E_m^{Mn^{4+}}$ ($La_{1-x}Sr_xMnO_3$), (b) $E_m^{Mn^{3+}}$ ($La_{1-x}Sr_xMnO_3$), (c) $E_m^{Mn^{4+}}$ ($La_{1-x}Ca_xMnO_3$), (d) $E_m^{Mn^{3+}}$ ($La_{1-x}Ca_xMnO_3$).

tration, is not linear, in contrast to A site migration, and is apparently independent of acceptor-dopant, at least for low dopant concentrations.

For the $La_{1-x}Sr_xMnO_3$ system we can compare our results with experimental work. Comparisons between calculated migration energies and experimental data are, however, seldom straightforward. The problem is that most experimental studies yield the activation energy of self-diffusion, E_a^X, which is the sum of the vacancy migration energy, E_m^X, and the energy associated with the change in defect concentration with temperature, E_d^X. From creep experiments on $La_{1-x}Sr_xMnO_{3+\delta}$ samples, Wolfenstine *et al.*[16] extracted activation energies for bulk self diffusion, which varied between 4 and 5 eV, but they were unable to say whether these values referred to lanthanum, strontium or manganese self-diffusion. From nonstoichiometry data,[5,6] we estimate E_d to be of the order of -1 eV for the temperature range in which the creep experiments were carried out (1150–1300 °C) for both A and B sites. E_d is negative for $LaMnO_{3+\delta}$ in this temperature range because δ, and hence the concentration of cation vacancies, decreases as the temperature is raised. We note incidentally that E_d will not necessarily take the same value at all temperatures. The formation of cation defects at high temperatures (possibly already at sintering temperatures) will be directly governed by Schottky disorder, and therefore E_d would be equal to $+E_S/5$. Thus for the creep experiments, where E_a is between 4 and 5 eV and E_d is *ca.* -1 eV, it appears, on consideration of the calculated migration energies for $La_{1-x}Sr_xMnO_3$ (*ca.* 5 eV), that lanthanum diffusion is the rate limiting process for creep. As calculated values of E_m^{Mn} were found to be higher than E_m^{La}, one could assume either that fast grain boundary diffusion of Mn takes place, or that the Mn vacancy migration energy is reduced by lanthanum vacancy mediation. The latter, as already noted, is only a tentative result, since we have not evaluated the entire energy profile for such a mechanism. Turning to the sintering experiments,[12–15] we find good agreement between our results and the conclusions of all the studies. Our assertion of La diffusion being rate limiting agrees with the conclusions of van Roosmalen *et al.*[14] and Stevenson *et al.*,[15] and is also consistent with the work of Katayama *et al.*[12] and Hammouche *et al.*,[13] since we found that the activation energies for La migration increase with Mn^{4+} concentration.

It would, of course, be preferable to compare our results with activation energies determined from experiments that probe the diffusion of a specific cation. Unfortunately, there are no such data for $LaMnO_{3+\delta}$, as mentioned earlier, but other perovskite oxides have been studied, of which $LaCrO_3$ is the most closely related. Akashi *et al.* obtained an activation energy of 4.98 eV for La diffusion in $LaCrO_3$ from solid state reaction experiments,[35] while Horita *et al.* employed SIMS to study the interdiffusion of acceptor dopant cations in a $La_{0.95}Sr_{0.05}CrO_3$–$La_{0.75}Ca_{0.25}CrO_3$ diffusion couple and found the activation energy of interdiffusion to be 3.30 eV.[36] Both these values are of the same order of magnitude as the calculated migration energies for A site cations in $La_{1-x}Sr_xMnO_3$ and $La_{1-x}Ca_xMnO_3$, although it must be remembered that the former contain E_d as well. Unfortunately, we cannot extract vacancy migration energies in this case since, in contrast to lanthanum manganite, cation vacancies are minority species and thus E_d can only be obtained by defect chemical modelling with knowledge of all the relevant equilibrium constants.

For $La_{1-x}Sr_xMnO_3$ the calculations indicate that $E_m^{La} \neq E_m^{Sr} \neq E_m^{Mn}$ and $E_d^{La} \neq E_d^{Mn}$. One would therefore expect the isothermal diffusivities of La, Sr and Mn to be different, and hence it is possible that under a thermodynamic potential gradient, kinetic demixing of an initially homogeneous sample will take place.[37] In SOFC's, the cathodes operate under an electrochemical potential gradient which may give rise to the degradation of the material over long periods of time. With regard to diffusion in real systems, such as SOFC cathodes, we would like to point out that planar defects may be important especially at intermediate temperatures. Grain boundaries may provide fast diffusion paths in ceramics, while in porous bodies preferential transport may well occur along surfaces.

Finally, we note that calculated oxygen vacancy migration energies for all the investigated cubic compositions lie between 0.45 and 0.72 eV. These are consistent with both experimental[38] and theoretical values.[22] As expected, they are also much lower than the calculated cation migration energies.

4 Concluding remarks

We have used atomistic simulation techniques to examine cation defect processes in $LaMnO_3$, processes which are relevant to the fabrication, utilisation and degradation of this material. The following results are noteworthy.

The calculated defect energies suggest that significant intrinsic disorder of the Frenkel or Schottky type is unlikely. In particular, interstitial defects are unfavourable, as expected from the close packed nature of the perovskite lattice.

The calculations also suggest that in the orthorhombic and

rhombohedral structures oxidative nonstoichiometry leads to the formation of cation vacancies on both La and Mn sites, though tending towards more La vacancies. This tendency is not a surprising result, since it is well known that the perovskite structure is capable of accommodating nonstoichiometry on the A site: the limiting case being that of ReO_3, in which the A site is completely empty.

Examination of cation transport in $LaMnO_3$ reveals that the La vacancy migration energy is about 4 eV, but increases with distortion from the cubic form. This increase is probably related to increased steric hindrance at the saddle point for the non-cubic structures. Simulations of A-site migration in $La_{1-x}Sr_xMnO_3$ and $La_{1-x}Ca_xMnO_3$ find the migration energy decreasing in the order $E_m^{La} > E_m^{Sr} > E_m^{Ca}$, and this is attributed to a combination of steric, electrostatic, and polarisability factors.

The lowest energy mechanism for Mn migration is found to be a curved path between adjacent Mn sites along the $<100>_{cubic}$ directions; the lowest value is 7.7 eV for the cubic structure. However, preliminary calculations suggest that the Mn vacancy migration energy is reduced substantially by the presence of a neighbouring La vacancy. Such migration mechanisms are currently under detailed investigation.

Acknowledgements

R.A.De S. would like to thank J. D. Gale, M. S. Read and A. Tücks for their assistance, W. Menesklou, K. Eberman and J. A. Kilner for stimulating discussions, and the Keramikverbund Karlsruhe Stuttgart (KKS) for financial support.

References

1 G. H. Jonker and J. H. Van Santen, *Physica*, 1950, **16**, 337.
2 N. Q. Minh, *J. Am. Ceram. Soc.*, 1993, **76**, 563.
3 R. M. von Helmholt, J. Wecker, B. Holzapfel, L. Schultz and K. Samwer, *Phys. Rev. Lett.*, 1993, **71**, 2331.
4 S. Jin, T. H. Tiefel, M. McCormack, R. A. Fastnacht, R. Ramesh and L. H. Chen, *Science*, 1994, **264**, 413.
5 J. H. Kuo, H. U. Anderson and D. M. Sparlin, *J. Solid State Chem.*, 1989, **83**, 52.
6 H. Tagawa, J. Mizusaki, H. Nambu, C. Nakao, H. Takai and H. Minamiue, in *Ceramic Oxygen Ion Conductors and Their Technological Applications*, British Ceramic Proc. vol. 56, The Institute of Materials, London, 1996, p. 113.
7 B. C. Tofield and W. R. Scott, *J. Solid State Chem.*, 1974, **10**, 183.
8 J. A. M. van Roosmalen, E. H. P. Cordfunke, R. B. Helmholdt and H. W. Zandberg, *J. Solid State Chem.*, 1994, **110**, 100.
9 J. F. Mitchell, D. N. Argyriou, C. D. Potter, D. G. Hinks, J. D. Jorgensen and S. D. Bader, *Phys. Rev. B*, 1996, **54**, 6172.
10 J. A. Alonso, M. J. Martínez-Lope, M. T. Casais, J. L. MacManus-Driscoll, P. S. I. P. N. de Silva, L. F. Cohen and M. T. Fernández-Díaz, *J. Mater. Chem.*, 1997, **7**, 2139.
11 Q. Huang, A. Santoro, J. W. Lynn, R. W. Erwin, J. A. Borchers, J. L. Peng and R. L. Greene, *Phys. Rev. B*, 1997, **55**, 14987.
12 K. Katayama, T. Ishihara, H. Ohta, S. Takeuchi, Y. Esaki and E. Inukai, *J. Ceram. Soc. Jpn. Int. Ed.*, 1989, **97**, 1324.
13 A. Hammouche, E. Siebert and A. Hammou, *Mater. Res. Bull.*, 1989, **24**, 367.
14 J. A. M. van Roosmalen, E. H. P. Cordfunke and J. P. P. Huijsmans, *Solid State Ionics*, 1993, **66**, 285.
15 J. W. Stevenson, P. F. Hallman, T. R. Armstrong and L. A. Chick, *J. Am. Ceram. Soc.*, 1995, **78**, 507.
16 J. Wolfenstine, K. C. Goretta, R. E. Cook and J. L. Routbort, *Solid State Ionics*, 1996, **92**, 75.
17 A. Weber, R. Männer, B. Jobst, M. Schiele, H. Cerva, R. Waser and E. Ivers-Tiffée, in *Proc. 17th Risø Int. Symp. Mater. Sci.*, *High Temperature Electrochemistry: Ceramics and Metals*, ed. F. W. Poulsen, N. Bonanos, S. Linderoth, M. Mogensen, and B. Zacharau-Christiansen, Risø National Laboratory, Roskilde, Denmark, 1996, p. 473.
18 J. D. Gale, *J. Chem. Soc.*, *Faraday Trans.*, 1997, **93**, 629.
19 *Computer Simulation of Solids*, ed. C. R. A. Catlow and W. C. Mackrodt, Lecture Notes in Physics 166, Springer-Verlag, Berlin, 1982.
20 C. R. A. Catlow, in *Solid State Chemistry—Techniques*, ed. A. K. Cheetham and P. Day, Clarendon Press, Oxford, 1987, p. 231.
21 B. G. Dick and A. W. Overhauser, *Phys. Rev.*, 1958, **112**, 603.
22 M. Cherry, M. S. Islam and C. R. A. Catlow, *J. Solid State Chem.*, 1995, **118**, 125.
23 B. Ammundsen, J. Rozière and M. S. Islam, *J. Phys. Chem.*, *B*, 1997, **101**, 8156.
24 A. Wold and R. J. Arnott, *J. Phys. Chem. Solids*, 1959, **9**, 176.
25 J. Rodríguez-Carvajal, M. Hennion, F. Moussa, A. H. Moudden, L. Pinsard and A. Revcolevschi, *Phys. Rev. B*, 1998, **57**, R3189.
26 M. S. Islam and L. J. Winch, *Phys. Rev. B*, 1995, **52**, 10510.
27 A. Chainani, M. Mathew and D. D. Sarma, *Phys. Rev. B*, 1993, **47**, 15397.
28 *CRC Handbook of Chemistry and Physics*, ed. R. C. Weast, M. J. Astle and W. H. Beyer, CRC Press, Boca Raton, Florida, 64th edn., 1983–1984.
29 J. H. Harding and N. J. Pyper, *Philos. Mag. Lett.*, 1995, **71**, 113.
30 S. D'Arco and M. S. Islam, *Phys. Rev. B*, 1997, **55**, 3141.
31 J. A. M. van Roosmalen, P. van Vlaanderen, E. H. P. Cordfunke, W. L. IJdo and D. J. W. IJdo, *J. Solid State Chem.*, 1995, **114**, 516.
32 J. A. Kilner and R. J. Brook, *Solid State Ionics*, 1982, **6**, 237.
33 H. W. King, K. M. Castelliz, G. J. Murphy and W. Manuel, *J. Can. Ceram. Soc.*, 1982, **51**, 1. Quoted by van Roosmalen *et al.*[31]
34 R. D. Shannon, *Acta Crystallogr.*, *Sect. A*, 1976, **32**, 751.
35 T. Akashi, M. Nanko, T. Maruyama, Y. Shiraishi and J. Tanabe, *J. Electrochem. Soc.*, 1998, **145**, 2090.
36 T. Horita, M. Ishikawa, K. Yamaji, N. Sakai, H. Yokokawa and M. Dokiya, *Solid State Ionics*, 1998, **108**, 383.
37 H. Schmalzried, *Chemical Kinetics of Solids*, VCH, Weinheim, 1995, p. 183.
38 R. A. De Souza and J. A. Kilner, *Solid State Ionics*, 1998, **106**, 175.

Paper 9/01512D